Knowledge-Based Systems 278 (2023) 110858

Contents lists available at ScienceDirect

Knowledge-Based Systems

journal homepage: www.elsevier.com/locate/knosys

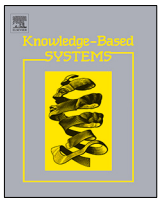

Adazd-Net: Automated adaptive and explainable Alzheimer's disease detection system using EEG signals

Smith K. Khare [a,*], U. Rajendra Acharya [b]

[a] Electrical and Computer Engineering Department, Finlandsgade 22, Aarhus University, 8200, Aarhus, Denmark
[b] School of Mathematics, Physics and Computing, University of Southern Queensland, Springfield, Australia

ARTICLE INFO

Article history:
Received 20 November 2022
Received in revised form 25 July 2023
Accepted 26 July 2023
Available online 29 July 2023

Keywords:
Alzheimer's disease detection
Electroencephalography
Brain region analysis
Explainable artificial intelligence
Adaptive wavelets

ABSTRACT

Background: Alzheimer's disease (AZD) is a degenerative neurological condition that causes dementia and leads the brain to atrophy. Although AZD cannot be cured, early detection and prompt treatment can slow down its progression. AZD can be effectively identified via electroencephalogram (EEG) signals. But, it is challenging to analyze the EEG signals since they change quickly and spontaneously. Additionally, clinicians offer very little trust to the existing models due to lack of explainability in the predictions of machine learning or deep learning models.
Method: The paper a novel Adazd-Net which is an adaptive and explanatory framework for automated AZD identification using EEG signals. We propose the adaptive flexible analytic wavelet transform, which automatically adjusts to changes in EEGs. The optimum number of features needed for effective system performance is also explored in this work, along with the discovery of the most discriminant channel. The paper also presents the technique that can be used to explain both the individual and overall predictions provided by the classifier model.
Results: We have obtained an accuracy of 99.85% in detecting AZD EEG signals with ten-fold cross-validation strategy.
Conclusions: We have suggested a precise and explainable AZD detection technique. Researchers and clinicians can investigate hidden information concerning changes in the brain during AZD using our proposed model. Our developed Adazd-Net model can be employed in hospital scenario to detect AZD, as it is accurate and robust.

1. Introduction

Dementia is one of the most typical forms of Alzheimer's disease (AZD), resulting in up to 80% of the cases [1]. AZD is chronic, starting with mild memory loss and potentially progressing to the loss of communication and environmental awareness. The brain regions responsible for thought, memory, and language are affected by AZD. It can significantly impair a person's capacity to carry out daily tasks. The estimated prevalence of dementia from all causes ranges from 8.7% in North Africa and the Middle East, 4.7% in Central Europe, and 6.4% in North America. More than 46 million people worldwide already suffer from dementia, and by 2050, that number is expected to rise to 131.5 million [2]. Women are about twice likely to develop AZD than men, however, men have a relatively shorter life span after the diagnosis [1]. AZD develops in a majority of people after the age of 65 and people living with the disease doubles every 5 years beyond the age of 65 [3]. Young individuals can also get AZD but it is uncommon. The socio-economical conditions also play a key role in the progression or development of AZD. Countries with low income have a higher prevalence of developing AZD than the developed economies. AZD is characterized by memory impairments, confusion with location, poor judgment, frequent changes in mood or personality, lack of concentration, unfounded suspicions about family, friends and professional caregivers, difficulty in speaking, swallowing and walking, etc [3]. Although AZD is incurable, early detection and diagnosis of AZD may allow patients to carry out their tasks normally and delay its progression. This demands an urgent need for an accurate and automated AZD detection system.

Numerous methods have been developed to detect and diagnose AZD. The techniques to diagnose AZD involve manual assessment, brain-imaging, and signaling. Manual assessment make use of mental status testing, neuropsychological tests, and interviews with friends and family [4]. Brain-imaging diagnosis of AZD include computerized tomography, Positron emission tomography, functional magnetic resonance imaging (fMRI), and magnetic resonance imaging [5,6]. Signaling-based AZD diagnosis make use of electroencephalogram (EEG) signals and magnetoencephalogram (MEG) signals [7]. However, manual assessment

* Corresponding author.
E-mail address: smith7khare@gmail.com (S.K. Khare).

https://doi.org/10.1016/j.knosys.2023.110858

is susceptible to bias, depends on experience of the experts, and time-consuming. Brain-imaging techniques provide detailed topology of the brain changes but are expensive, require extra recordings, and may be prone to radiations. Signaling techniques are fast, portable, provide minute temporal resolution, and cost effective. MEG signaling require dedicated room for recording, the equipments are costly, and bulky. The underlying limitations of various techniques and modalities makes EEG a better choice for AZD detection. Also, EEG signals are globally accepted and explored for the detection of numerous brain conditions [8–11]. Hence, we used EEG signals in our analysis for the detection of AZD. Various studies have used EEG signals for AZD detection and are discussed in the next section.

2. Related work

Over time, many EEG-based studies have been reported by researchers for automated recognition of AZD (and normal cognition (NC)). In this section, a detailed description of the recently developed AZD detection methods are explored. The description includes EEG dataset, signal analysis methods, validation strategy, and decision-making techniques. Table 1 presents the summary of the existing state-of-the-art (SOTA) techniques used for AZD detection using EEG signals.

2.1. Summary of the existing models

Authors have used relative band power (RBP), spectral analysis, different entropies like approximate (ApEN), permutation (PEN), sample (SampEN), spectral (SpecEN), Shannon (SHEN), quadratic sample entropy (QSE), fuzzy (FEN), multiscale entropy (MSE), nonlinear features including Lampel Ziv complexity (LZC), correlation dimension, Hjorth complexity (HC), auto mutual information (AMI) and Lyapunov exponents combined to detect AZD [12–19]. Authors have extracted linear and nonlinear features, decomposition-based AZD detection which includes tunable Q wavelet transform (TQWT), empirical mode decomposition (EMD), rational dyadic low-complexity orthogonal filter banks with vanishing moments (LCOWFBs-v), and wavelet packet analysis (WPA) with traditional machine learning (ML)-techniques like decision tree (DT), random forest (RF), support vector machine (SVM) including least square SVM (LSSVM), k-nearest neighbors (KNN), artificial neural network (ANN), ensemble family classifiers (boost, bagged (EBT), and random undersampling) [20–24]. In addition, time, frequency, and time–frequency analysis combined with ML-based techniques have been explored for the detection of AZD using short-time Fourier transform (STFT), continuous wavelet transforms (CWT), primate brain pattern (PBP), discrete wavelet transform (DWT), and spectral analysis [25–32]. Authors have also explored deep learning (DL) techniques for the automatic detection of AZD and its stages using convolutional neural networks (CNNs), variational auto-encoders, long-short term memory (LSTM) networks, recurrent neural networks, deep dynamic residual networks, generative adversarial networks, deep pyramidal CNN (DPCNN), and variational auto encoder [33–45]. The EEG signals are transformed into images to obtain the time–frequency representations using stationary wavelets, CWT, and STFT. In some cases, principal component analysis (PCA), spectral analysis (fast Fourier transform), and correlation analysis have been explored for AZD detection [33–45].

2.2. Challenges with existing models

Choosing an appropriate scaling function for nonlinear features is difficult. There is difficulty in the selection of window type for STFT and its length. Appropriate choice of type of mother wavelet for wavelet-based analysis are few limitations of the existing methods. Also, the filtering techniques suffer band overlapping and fast Fourier transform lacks time–frequency localization. The EEG signals are nonlinear which makes its analysis difficult.

2.3. Available scope for AZD detection

The scope available for the accurate detection of AZD are given below:

- **Adaptive signal analysis:** The existing feature extraction techniques use a predefined basis to analyze the spontaneously varying EEG signals which may not extract representative information.
- **Selection of optimal feature:** There is no standard technique or tool that describes the requirement of minimal number of features required for maximizing the system performance.
- **Computational cost:** DL techniques enable automatic feature extraction and classification but demands higher memory requirements, computationally expensive, and timely.
- **Explainability:** It is introduced to aid in interpreting the developed models using SHapley Additive exPlanations (SHAP), Local Interpretable Model-agnostic Explanations (LIME), Gradient-weighted Class Activation Mapping (Grad-CAM), Guided Grad-CAM, and Expected Gradients methods [46].

2.4. Thesis of the paper

The proposed work explores the aforementioned issues to narrow down the research gaps in the detection of AZD using EEG signals. Therefore, an adaptive flexible analytic wavelet transform (AFAWT) has been proposed for the automatic selection of tuning parameters to decompose the EEG signals into subbands (SBs). It is accomplished using an evolutionary artificial hummingbird optimization algorithm (AHOA) to minimize the root mean square deviation (RMSD) of decomposition [47]. Feature engineering and channel play a crucial role in brain disorder detection. In this study, we have performed the channel and feature analysis to find the most significant channel and an optimal number of features required for accurate detection of AZD. The explainable boosting machine (XBM) with three explainers are used to explain individual and overall predictions [48]. The effectiveness of the proposed Adazd-Net (adaptive Alzheimer's disease detection network) is evaluated by comparing performance matrices using holdout, leave one subject out (LOSO), and 10-fold cross-validation (CV) techniques. We have compared our results with the existing state-of-the-art (SOTA) models using the same AZD EEG dataset. Finally, we have evaluated five performance matrices: accuracy (ACCY), precision (PRCS), sensitivity (SNSY), specificity (SPCY), and F1-score to study the effectiveness of our developed Adazd-Net model. The main contributions of our developed model are listed as follows:

- The EEG signals are highly varying and hence difficult to analyze [49]. Therefore, we have developed an AFAWT to automate the tuning parameters to obtain adaptive SBs.
- AZD destroy neurons and their connections in parts of the brain involving memory [5,27]. Therefore, we have conducted brain region analysis at different lobes to find significant regions contributing to AZD.

Table 1
Summary of previous studies conducted on automated AZD detection using EEG signals.

Author(s) & Year	Method	Technique	Validation strategy	Dataset (Subjects)
[12] & 2022	RBP, SpecEN, and HC	SA	LOSO	AZD:12 NC:9
[13] & 2022	PEN, SampEN, and LZC	SA	–	AZD1:17 AZD2:16 NC:16
[14] & 2006	MSE	SA	–	AZD:12 NC:11
[18] & 2006	SpecEN and SHEN	SA	–	AZD:12 NC:11
[15] & 2006	ApEN and Spectral analysis	SA	–	AZD:10 NC:08
[16] & 2008	ApEN and AMI	SA	–	AZD:11 NC:11
[19] & 2015	QSE	SA	–	AZD:11 NC:11
[17] & 2018	FEN	SA	–	AZD:12 NC:11
[26] & 2019	STFT, CWT, modulation features, spectral features, and amplitude modulation rate of change	traditional ML	LOSO	AZD1:15 AZD2:19 NC:20
[25] & 2017	Spectral, coherence, and amplitude modulation features	traditional ML	10-fold & LOSO	AZD1:15 AZD2:19 NC:20
[27] & 2022	PBP and TQWT	traditional ML	10-fold & LOSO	AZD:12 NC:11
[20] & 2021	SpecEN and KMC	traditional ML	10-fold	AZD:12 NC:11
[21] & 2022	TQWT (TSEN, REN, KFD, and KURT)	traditional ML	10-fold	AZD:12 NC:11
[22] & 2022	EMD (Hjorth parameters)	traditional ML	10-fold	AZD:12 NC:11
[23] & 2022	WPA and statistical features	traditional ML	10-fold	AZD:12 NC:11
[24] & 2023	LCOWFBs-v (HFD and KFD features)	traditional ML	10-fold	AZD:12 NC:11
[28] & 2022	DWT and statistical features	traditional ML	10-fold	AZD1:22 AZD2:31 NC:35
[30] & 2022	Filtering	traditional ML	10-fold	AZD:20 NC:20
[29] & 2022	Band power ratio, complexity, functional connectivity, and CWT	traditional ML	5-fold	AZD:72 MCI:116 NC:113
[31] & 2022	PSD with spectrogram and filtering	traditional ML	10-fold	AZD:49 MCI:37 NC:23
[32] & 2020	Filtering and brain connectivity	traditional ML	5-fold	AZD:30 NC:30
[33] & 2022	Robust PCA and multiscale PCA	DL	Holdout	AZD:20 NC:15
[34] & 2022	Stationary wavelet transform	DL	Holdout	AZD:49 MCI:39 NC:23
[35] & 2022	Correlation analysis (Granger causality test, Pearson's, and Spearman's correlation)	DL	Holdout	AZD:24 NC:24
[36] & 2022	Rhythm analysis using filtering	DL	2-fold	AZD:1 NC:8
[37] & 2022	Filtering	DL	5-fold	AZD:11 NC:16
[38] & 2021	CWT with statistical features	DL	Holdout	AZD:64 MCI:64 NC:64
[39] & 2022	CWT (Mexican hat)	DL	5-fold	AZD:63 MCI:56 NC:61
[40] & 2022	Synchronous-domain analysis	DL	5-fold	AZD:30 NC:30
[41] & 2019	FFT with spectral dimension	DL	Holdout	AZD:4 MCI:4 NC:4
[42] & 2021	CWT (Morse wavelet)	DL	10-fold	AZD:52 MCI:37 NC:52
[43] & 2023	FFT (Fourier coefficient)	DL	5-fold	AZD:49 MCI:37 NC:14
[44] & 2023	PSD and statistical features	DL	Holdout	AZD:59 MCI:7 NC:102
[45] & 2023	FFT with PSD	DL	Holdout	AZD:137 NAZD:594

TSEN — Tsallis entropy, REN — Renyi entropy, KFD — Katz's fractal dimension, HFD — Higuchi fractal dimension
KURT — Kurtosis, SA — Statistical analysis, NAZD — Non AZD.

- Neurologists find it difficult to trust the decision made by automated models due to lack of explainability. Therefore, we have presented an explainable artificial (XAI) model to explain individual and overall predictions of the developed model using LIME, SHAP, and Morris Sensitivity (MS).

The reminder of this paper is structured as follows. A brief description about the EEG dataset and developed model are presented in Section 3. The results are given in Section 4. The results are discussed and compared with the SOTA techniques are presented in Section 5. Finally, the conclusion and future directions are provided in Section 6.

3. Methodology

The methodology of the proposed work is partitioned into four subsections. First section highlight the EEG data used to evaluate the proposed model, second subsection describes the developed

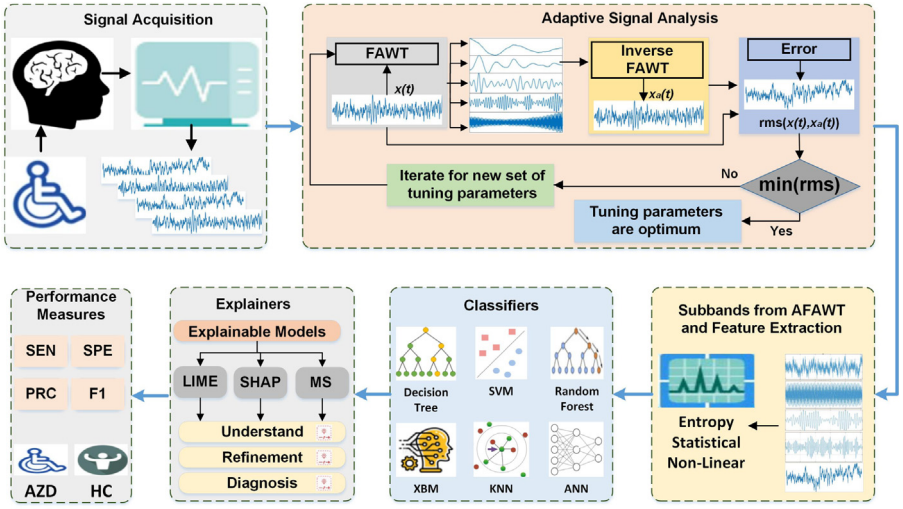

Fig. 1. Graphical overview of the proposed Adazd-Net.

Table 2
Summary of the class-wise distribution of AZD and NC subjects.

Class	NC	AZD
Total subjects (23)	11	12
Males (12)	7	5
Females (11)	4	7
Age (mean±std)	72.8 ± 6.1 years	72.8 ± 8 years
MMSE score (mean±std)	30 ± 0	13.1 ± 5.9
Total signals (663)	263	400

adaptive wavelet i.e. AFAWT, third subsection provides the details about featureset, and final subsection presents the explainable ML model. The graphical implementation steps of the developed adaptive and explainable AZD detection model is shown in Fig. 1.

3.1. Dataset

The EEG dataset used for the experimental analysis of the proposed model composed of 23 subjects. The dataset comprised of 11 subjects with NC and 12 subjects having AZD. The subjects belonging to both the classes (NC and AZD) were recruited from the Alzheimer's Patients' Relatives Association of Valladolid. The 16-channel (Fp_1, Fp_2, P_3, P_4, C_3, C_4, O_1, O_2, T_3, T_4, T_5, T_6, F_3, F_4, F_7, and F_8) EEG recorder (Study room 2.3.411 EEG system) built in-accordance with international 10–20 system have been used for the signal acquisition [50]. The severity of dementia in the AZD patients has been determined using a Mini-Mental State Examination (MMSE) method [51]. An EEG recording study has been approved by the Hospital Clinico Universitario de Valladolid (Spain) Ethics Committee. All NC participants and all those who are care-giving for AZD patients have given written approval to participate. The Folstein's literature describes a maximum MMSE score of 30 [51]. Additionally, dementia is classified as mild between the ages of 20 and 24, moderate between 13 and 20, and severe for score of 12 and below. Among 12 AZD patients, 5 were reported severe dementia with a score of less than 12 while the remaining had moderate dementia having a score of 13.1. All the NC subjects did not have or history of dementia or any neurological disorders. The details about the AZD dataset created by the Alzheimer's Patients' Relatives Association of Valladolid is shown in Table 2. The dataset is publicly available and its details can be found in [50,52].

The EEGs were captured at a sampling rate of 256 Hz for more than 5 min. Subjects were awake, with their eyes closed in a rested condition during recording. The specialized physician was recruited to choose the EEG epochs with least electromyography activity, electrooculographic artifacts, and movements. Finally, the EEG data was segmented into 5s epoch with 1280 samples. In this paper, we have also performed the brain-region analysis in various lobes. We have constructed four lobes with different combination of channels. The frontal region (FR) is comprised of six channels namely, Fp_1, Fp_2, F_3, F_4, F_7, and F_8, central region (CR) with C_3, C_4, T_3 and T_4 channels, parietal region (PR) comprised of channels P_3, P_4, T_5, and T_6, and occipital region (OR) with two channels O_1 and O_2.

3.2. Adaptive Flexible Analytic Wavelet Transform (AFAWT)

FAWT is an advanced form of DWT with time–frequency covering due to which it has gained a lot of attention in bio-signal analysis [53,54]. The FAWT incorporates Hilbert transform pairs of atoms, making it useful for analyzing signals with oscillations. It uses an iterative filter bank consisting of two highpass (HPF) and one lowpass (LPF) filter. The frequency response of HPF is represented by [55]

$$H_p(\omega)=\begin{cases}\sqrt{t_{p_1}t_{p_2}}, & |\omega|<\omega_p,\\ \sqrt{t_{p_1}t_{p_2}}\phi((\omega-\omega_p)(\omega_s-\omega_p)^{-1}), & \omega_p\le\omega\le\omega_s,\\ \sqrt{t_{p_1}t_{p_2}}\phi((\pi-\omega+\omega_p)(\omega_s-\omega_p)^{-1}), & -\omega_s\le\omega\le-\omega_p,\\ 0, & |\omega|\ge\omega_s.\end{cases} \tag{1}$$

The frequency response of LPF is denoted by [55]

$$L_p(\omega)=\begin{cases}\sqrt{t_{p_3}t_{p_4}}\phi((\pi-(\omega+\omega_0))(\omega_1-\omega_0)^{-1}), & \omega_0\le\omega\le\omega_1,\\ \sqrt{t_{p_3}t_{p_4}}, & \omega_1\le\omega\le\omega_2,\\ \sqrt{t_{p_3}t_{p_4}}\phi((\omega-\omega_2)(\omega_3-\omega_2)^{-1}), & \omega_2\le\omega\le\omega_3,\\ 0, & \omega\in[0,\omega_0)\cap(\omega_3,2\pi).\end{cases} \tag{2}$$

The boundary conditions for LPF and HPF frequency responses are [55]

$$\omega_p=\frac{(1-\hat{\beta})\pi+\epsilon}{t_{p_1}};\quad \omega_s=\frac{\pi}{t_{p_2}};\ \omega_0=\frac{(1-\hat{\beta})\pi+\epsilon}{t_{p_3}};\\ \omega_1=\frac{t_{p_1}\pi}{t_{p_2}t_{p_3}};\quad \omega_2=\frac{\pi-\epsilon}{t_{p_3}};\ \omega_3=\frac{\pi+\epsilon}{t_{p_3}}. \tag{3}$$

The condition required to perfect reconstruction is defined by [55]

$$|\phi(\pi-\omega)|^2+|\phi(\omega)|^2=1. \tag{4}$$

For perfect reconstruction, the function $\phi(\omega)$ must satisfy [55]

$$\phi(\omega)=0.5\times[1+\cos(\omega)][2-\cos(\omega)]^{1/2},\quad \text{for } \omega\in[0,\pi]. \tag{5}$$

The positive constraint $\hat{\beta}$ and ϵ are represented by [55]

$$\begin{aligned} 1-\frac{t_{p_1}}{t_{p_2}}\le\hat{\beta}\le\frac{t_{p_3}}{t_{p_4}};\\ \epsilon\le\Big(\frac{t_{p_1}-t_{p_2}+\hat{\beta}t_{p_2}}{t_{p_1}+t_{p_2}}\Big)\pi;\\ \hat{\beta}=\frac{2}{Q_F+1}. \end{aligned} \tag{6}$$

The redundancy rate of the transform is represented by [55]

$$\mathrm{r}\approx(t_{p_3}/t_{p_4})\frac{t_{p_2}}{t_{p_2}-t_{p_1}}. \tag{7}$$

Finally, the quality factor of the transform is defined as [55]

$$Q_F=\frac{\omega_0}{\Delta\omega}. \tag{8}$$

The FAWT matlab tool box for signal decomposition is available at (https://web.itu.edu.tr/ibayram/AnDWT/). The above mathematical formulations show that tuning parameters, according to the FAWT formulation, regulate the number of oscillations in the wavelet. The produced wavelet for a particular quality factor will have the same amount of oscillations for different decomposition levels. The form of these wavelets will change when the FAWT tuning parameters are changed. Thus, for decomposing an oscillatory EEG signal into SBs, require to define quality factor, redundancy rate, and level of decomposition. The values of redundancy rate and quality factor are controlled by the tuning parameters ($t_{p_1}, t_{p_2}, t_{p_3}, t_{p_4}$). Therefore, for efficient analysis and synthesis these parameters are required to be set precisely. Inaccurate selection of these tuning parameters may result in improper synthesis and result in degraded system performance. Manual tuning of these parameters is time-consuming and often prone to human errors. To overcome the problem of empirical and experimental parameter setting, we have designed AFAWT method. AFAWT is a combination of FAWT and AHOA to automate the tuning parameters by reducing the cost function of RMSD. The AHOA is inspired by the flight skills and intelligent foraging strategies of hummingbirds in nature. AHOA uses three skills of hummingbirds: foraging strategies, including axial, diagonal, and omnidirectional flights [47]. In our work, we have used a cost function of RMSD to select the optimum tuning parameters. The cost function is given by

$$RMSD=\sqrt{\frac{\sum_{n=1}^{N}(y_n-y_n^a)^2}{N}}. \tag{9}$$

where y_n and y_n^a are the original and approximated signals and N are the number of samples in a SB. The optimization algorithm involves four steps: (i) initialization phase, (ii) guided foraging, (iii) territorial foraging, and (iii) migration foraging. The detailed operations performed are presented in Appendix A. In our proposed model, the tuning parameters required for decomposition are the variables and the fitness or cost function is RMSD. Once the optimum tuning parameters are obtained using AHOA, then they are used for decomposing the EEGs to get representative SBs for further analysis.

3.3. Features

Features play a crucial role in automated decision-making. A user is available with a pool of features including time, frequency, nonlinear, entropy, and time–frequency. But selecting appropriate features for decision-making is a tedious task. Also, the features must be selected such that it performs equally and effectively for variations in system topology. Therefore, in our proposed framework we have explored statistical, nonlinear, and entropy features to test our model. A total of 85 features are extracted from the SBs of NC and AZD signals using AFAWT. There are 21 statistical, 22 entropy, and 42 nonlinear features. The details about features used in our work is available in [49,56–60]. The complete list and abbreviation of these features are provided in Appendix in Tables B.7, C.8, and D.9.

3.4. Decision making

The section investigates how the proposed framework is developed for predictions and explains the underlying result. The XBM model is used to determine if the EEG is NC or AZD. The explainers also give explanations for the ML model's decisions for individual and overall predictions.

3.4.1. Classifier

ML models make predictions using a variety of fitness functions. These ML models provide a classification report of the model's overall performance in terms of performance parameters, a confusion matrix, and receiver operating characteristics. The overall performance of the model serves as a representation of the corresponding mathematical behavior or approach. It does not, however, convey any information about predictions or a justification for how they are made. To overcome this, we used an XBM model that provides information on interpretations specific to the model, a precise justification of gains or losses, and model analysis following training. In addition of this, we have also provided a comparative analysis of the XBM model with benchmark classification techniques like SVM, KNN, decision tree (DT), ANN, and RF [61]. Explainers (post hoc technique) are model agnostic, which provide model analysis after training. Since it relies on having access to the model's inputs and outputs, it can only offer approximations of explainability. The XBM model is combined with three explainers i.e. LIME and SHAP for explaining local prediction and MS for exploring global predictions. The mathematical expression for generalized additive model of XBM is denoted by [48]

$$h(\mathcal{E}[x])=\beta_0+\sum f_j(z_j). \tag{10}$$

The above equation is transformed into pairwise interactions represented by

$$h(\mathcal{E}[x])=\beta_0+\sum f_j(z_j)+\sum f_{j,k}(z_j,z_k), \tag{11}$$

where the dependent variables are denoted by z_j, z_k, intercept is denoted by β_0, and x are the observations. XBM's feature function f_j is trained using either boosted gradient or bagging algorithm. The graphical illustration of traditional ML and explainable ML model is shown in Fig. 2.

3.4.2. Explainers

- **LIME**: It modifies samples and original data to produce a new data to explain local predictions of ML model [62]. The interpretable weighting on which LIME trains depends on how close the sampled examples are to the instance of interest. Although a strong global approximation is not necessary, the learned model should locally be a reasonable approximation of the ML model's predictions.

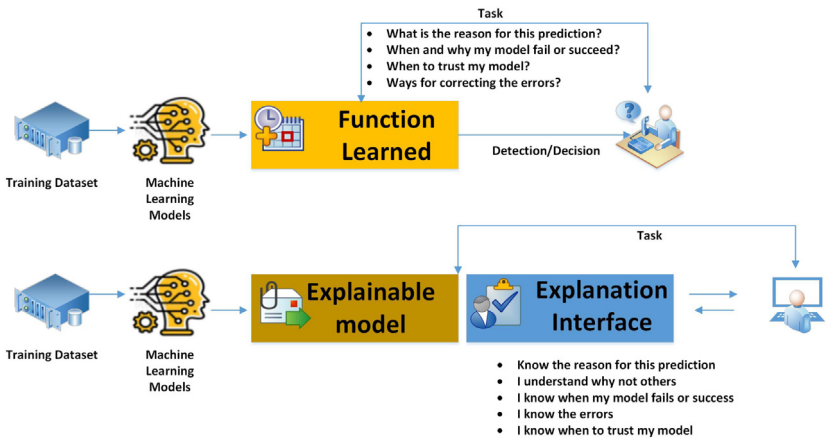

Fig. 2. Difference between traditional ML and explainable ML models.

- **SHAP**: According to coalitional game theory, Shapley values are computed using SHAP explanation method [63]. Players in a coalition are the feature values of a data instance. Utilizing Shapley values, may spread the prediction across the attributes in an equitable manner. The Shapley values presented as an additive feature attribution method using a linear model.
- **MS**: It detects whether the input data is relevant for further analysis using global sensitivity analysis [64,65]. It takes one input at a time that modifies each level in every run.

4. Results

The paper investigates adaptable and explainable methods for detecting AZD in EEG data. It is extremely challenging to model the behavior of EEG signals that change spontaneously. As a result, we designed AFAWT to minimize the RMSE and extract the meaningful information from the AZD and NC EEGs. Using AHOA, the AFAWT generates recognizable SBs from the EEG signals. The cost function of RMSD is minimized for the optimal value of tuning parameters in each EEG epoch of NC and AZD. The experimental setup is maintained uniformly for both classes (NC and AZD). The number of iterations and search agents are empirically selected as 50 and 80. The tuning parameters for each EEG signal is labeled as optimum if the RMSD is minimum. The optimal tuning parameters obtained for each EEG epoch of both the classes are used to decompose the respective EEGs into their corresponding SBs. Table 3 provides the summary of average RMSD obtained using AFAWT for NC and AZD classes. To evaluate the effectiveness of the developed AFAWT, we have compared the errors obtained for AFAWT with traditional FAWT. The tuning parameters of FAWT are selected empirically for NC and AZD EEG signals and maintain uniformly. We have selected the value of $p = 3, q = 5, r = 2, s = 3$, and $J = 5$ empirically for FAWT. The table demonstrates that the developed AFAWT offers the least value of cost function, demonstrating its superior synthesis property. The results of Table 3 motivate us to use the optimal tuning parameters for further analysis. The generated SBs of AFAWT are used to extract numerous features. The features are categorized into three categories i.e. statistical features (21 nos.), entropy features (22 nos.), and nonlinear features (42 nos.). We have fused the features (85) of all 16 channels ($85 \times 16 = 1360$). The total signals for both classes are combined to get an input feature matrix of dimension 663×1360. As stated earlier, 400 instances belong to AZD category while 263 are the instances representing NC.

Table 3
Mean value of RMSD obtained using AFAWT.

Method	NC	AZD
FAWT	0.532	0.374
AFAWT	2.47×10^{-6}	1.95×10^{-6}

The classification report obtained for each SB using the XBM classifier is presented in Fig. 3. To evaluate the effectiveness of the XBM classifier we have compared the ACCY performance for each SB with five distinct benchmark classifiers. It is important to mention that the classifier parameters are fixed for each SB. The maximum number of splits for DT is taken as 10 with Gini's diversity index split criteria. A medium-sized ANN model is used with a layer size of 10, ReLU activation function, and 1000 maximum iterations. The Gaussian kernel with size of 36 is used for SVM while a number of neighbors are chosen as 5 for the weighted KNN model. The classification is performed using a k-fold CV technique with k = 10. As different classification algorithms work on different fitness functions, there is a possibility of bias in the decision given by the classifiers. To eliminate the possibility of bias, we have scaled down the feature values to a finite range using z-score normalization. The results shown in Fig. 3 demonstrate that XBM is the best performing classifier. The highest ACCY of 99.85% is obtained in SB-7 while the least ACCY of 83.71% in SB-3 using the DT classifier. DT classifier produces the least performance due to its poor ability to draw distinguishable decision boundaries for NC and AZD classes. The ACCY in SB-7 and SB-5 is more concentrated depicting their effectiveness in the detection of AZD. SB-7 generates more representative and distinguishable characteristics of AZD and NC EEGs which are more accurately classified than other SBs. Except DT, SB-1 turns out to be the least effective classifier. As a result, the features (of NC and AZD) generated in SB-1 overlap, which reduces classification accuracy. The XBM classifier is used for further investigations of the developed model because the ACCY report demonstrates that it outperformed other classifiers.

The EEG acquisition system consists of several channels placed throughout the scalp. The human brain is split into several areas, including the prefrontal, frontal, parietal, occipital, and central. These brain regions are responsible for distinguishing and performing various tasks [66]. The abnormal changes captured by these lobes during the AZD may provide detailed insight into the brain topology. Therefore, we have performed the brain region analysis for frontal, central, occipital, and parietal region. The ACCY score obtained for FR, PR, CR, and OR is 99.25%, 96.23%, 97.24%, and 93.85%, respectively. Thus, the electrodes in FR region

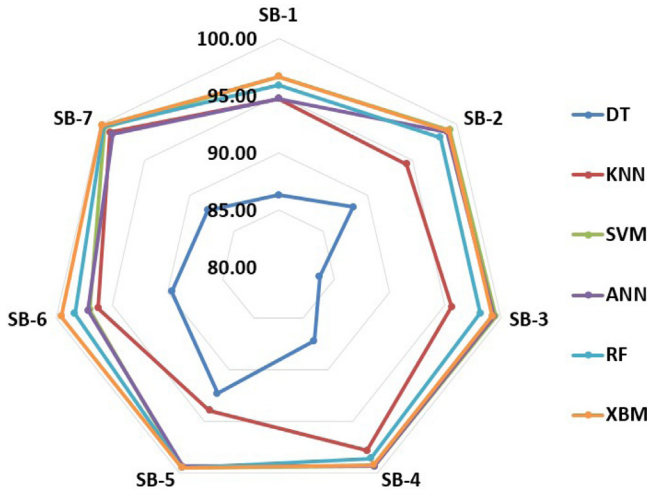

Fig. 3. Subband-wise accuracy variation for the benchmark classification techniques.

(responsible for personality and emotions, thinking skills, and controlling movement) captures detailed changes during AZD enabling higher possibilities of detecting AZD. In contrast, OR responsible for recognition of shapes and colors is least affected due to which it has resulted in the least accuracy. To get more insight into our developed model, we have evaluated five performance matrices for combined features using ten-fold CV, LOSO, holdout, and FR. The summary of performance report obtained for different combination is shown in Table 4. It is evident from the Table 4 that holdout validation (90% data for training and 10% data for testing) has provided an ACCY of 98.51%, while SNSY of 100%. The SNSY, SPCY, PRCS, and F1-score for 10-fold CV is 99.75%, 100%, 100%, and 99.88%, respectively. The LOSO validation has yielded the least performance with an ACCY, SNSY, SPCY, PRCS, and F1-score of 91.3%, 85.71%, 100%, 100%, and 93.21%, respectively. The performance report generated by Adazd-Net model shows that our developed model is effective and accurate in different scenarios. The analysis performed till this point has used all the features. According to the brain region assessment, the FR is the most informative lobe in the identification of AZD. However, it remains unclear which channel and feature generates distinguishable information for AZD detection. As a result, we conducted the statistical and ACCY analysis for each channel utilizing all features. Fig. 4 illustrates the channel rank obtained using univariate analysis and Table 5 shows the ACCY for each channel. It is seen from Fig. 4 that F_3 indicates the most discriminant properties followed by P_3, O_2, C_4, and Fp_2. On the other hand, channels F_7 and T_4 indicates the overlapping characteristics of AZD and NC EEGs. The channel-wise analysis show that the F_3 has obtained 98.94% surpassing the performance of all other channels. The other channels in FR i.e. Fp_1 and Fp_2 are second and third best with the ACCY score of 98.64%. T_4 channel has generated the minimum ACCY score of 91.25% indicating least contribution in the detection of AZD. The channel-wise analysis proves that in the frontal lobes, the most contributing features channels are F_3, Fp_1, and Fp_2.

Till now our model shown that frontal lobe with $F3$ channel contributes the most to detect the changes in the AZD and NC EEGs. However, it is still unclear the number of features needed to obtain the highest system performance. Therefore, to scale down the feature matrix from 85 to optimum number, we have performed univariate analysis on the features of F_3 channel. With the SA shown in Fig. 5, we have found the rank of each feature indicating the highest discrimination ability. Using the combination of the feature rank matrix, we have fused one feature at a time (based on the rank) to the most significant feature (MVTSR). Using this fused feature matrix of channel F_3 we have evaluated the ACCY score for each combination. Fig. 6 indicates the variation in ACCY score with different feature combination. It is evident from the figure that as the number of feature increases the ACCY score is also rises. The ACCY obtained using the most discriminant nine features is maximum i.e. 96.98% and decreases thereafter. Hence, our developed model produces maximum detection rate with only nine features of F_3 channel. The topographic maps developed shown in Fig. 7 indicate the accuracy and feature scores of various channels. The figures show that frontal region particularly channels F_3, Fp_2, and Fp_1 have generated discriminable characteristics have yielded the highest performance. Similarly, the channels C_4, P_3, and O_1 in central, parietal, and occipital regions have generated discriminable characteristics.

Finally, we have used a black-box approach to explain the predictions made by our employed ML model. LIME and SHAP techniques are used to explain the individual predictions made by our developed model and Morris sensitivity to explain the overall decisions of the developed model. The explanations for individual classification with channel and features provided by LIME are shown in Fig. 8 and Fig. 9, respectively. It is evident from Fig. 8 that the MVTSR feature has the highest contribution to the successful prediction of AZD and NC EEG epochs. EWL feature is placed in second position for the predictions of EEG epochs. In addition to this, other features like LTKEO, NZR SpecEN, SurEN, etc., have also shown significant contribution in the decision-making. Similarly, Fig. 9 presents the summary of channel contributions in individual predictions using LIME explainability. The graphical representations provided by LIME show that channel frontal channel especially F_3 has been the crucial characteristic for the decision-making of the classifier model.

We have also employed SHAP explainability to our ML model for further explaining the decisions. Figs. 10 and 11 provide the explanations given by SHAP for features and channels. It is again confirmed from these figures that the MVTSR, ACCSR, EWL, LTKEO, SpecEN, and SurEN are the most consistent features that have contributed for accurate classifications. Similarly, it is seen from the channel-level SHAP explanations that the F_3 channel is most significant and consistent in making individual predictions. In addition, the channels in FR i.e. Fp_1, Fp_2, F_7, and F_8 also contribute to making predictions. The SHAP analysis also confirms that channels in the parietal lobe i.e. P_3 and P_4 along with central lobe channels are also significant for predicting AZD. Finally, Morris sensitivity is used to explain the global prediction made by the ML model. Fig. 12(a) and (b) provides the explainability provided by Morris sensitivity analysis for channels and features. Convergence indices of 0.096 and 0.122 have been obtained for channels and features. The global explainability shows that channels F_3 and $Fp1$ contribute most to overall predictions, whereas for features MVTSR and EWL are the most significant global predictors. The analysis performed on channel and feature using SA, performance analysis, and explainability confirms the importance of highly contributing channels and features. Thus our model is robust, consistent, accurate, and explainable for making individual and global predictions.

5. Performance comparison

Table 6 shows the summary of the performance comparison with existing SOTA techniques using the same dataset. The comparison report includes the signal analysis techniques, classifiers,

Table 4
Performance measures(%) obtained for different combinations.

Validation strategy	ACCY (%)	SNSY (%)	SPCY (%)	PRCS (%)	F1-score (%)
10-fold	99.85	99.75	100	100	99.88
Frontal Region	99.25	98.86	99.24	99.25	99.37
Holdout	98.51	100	96.88	97.29	98.63
LOSO	91.30	85.71	100	100	92.31

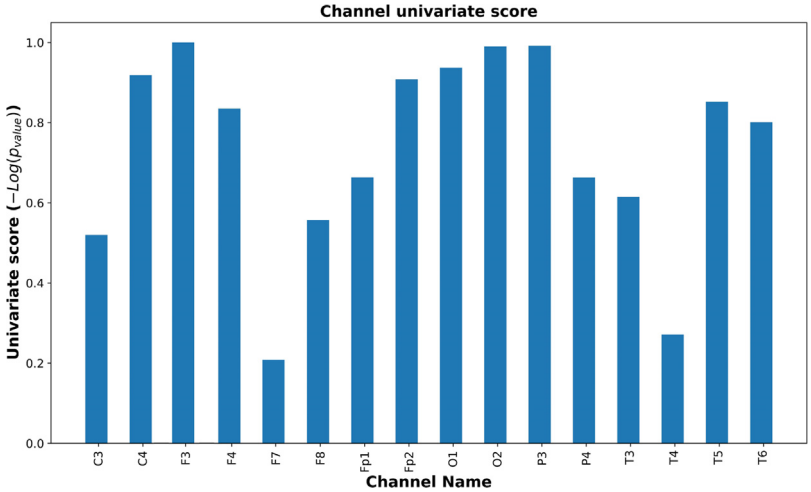

Fig. 4. Channel rank obtained using univariate analysis.

Table 5
Channel-wise accuracy score in SB-7 using XBM classifier with all features.

Channel	**C3**	**C4**	**F3**	**F4**
ACCY (%)	93.06	95.32	98.94	97.36
Channel	**F7**	**F8**	**Fp1**	**Fp2**
ACCY (%)	94.72	93.67	98.64	98.64
Channel	**O1**	**O2**	**P3**	**P4**
ACCY (%)	95.48	94.87	96.38	93.21
Channel	**T3**	**T4**	**T5**	**T6**
ACCY (%)	94.12	91.25	93.97	93.82

performance matrices, and validation techniques employed. The methods in [14–20] have used extraction of features directly from EEG epochs. EEG being highly non-stationary, analysis of features extracted from EEG limits the system's performance. Therefore, accurate analysis is required to find the hidden and representative characteristics to obtain desired performance using decomposition techniques. The research groups Puri et al. [20–24] and Dogan et al. [27] explored signal decomposition analysis using DWT, EMD, LCOWFBs-v, and TQWT. Decomposing techniques like DWT, LCOWFBs-v, and TQWT splits the signal into components to extract hidden information. But wavelet-based decomposition is required to provide the type of wavelet and define tuning parameters which are difficult to decide for rapidly varying EEG. EMD is data-driven and does not require any basis function, but its performance is limited due to mode mixing and generation of numerous intrinsic mode functions. Also, existing methods report a very high classification rate, but it fails to explain the classifier's decision. In addition, the existing models do not provide information about the number required for maximizing the system performance. In our proposed model we have tried to narrow down the above-mentioned research gaps using adaptive and explainable decision-making for the detection of AZD using EEG signals. The performance of our developed explainable model has surpassed the performance of the existing models with an ACCY, SNSY, SPCY, PRCS, and F1-score of 99.85%, 99.75%, 100%, 100%, and 99.88%. Our developed Adazd-Net model successfully targeted the following characteristics which were lacking in the SOTA models. It is noteworthy to mention that the authors used fewer subjects to develop the methods reported in [15,16,19].

- **Brain lobes analysis:** The human brain performs a variety of functions that come from different regions of the brain. The most impacted lobe or region of the brain during AZD can be identified by analyzing these brain regions. The most important lobe may be identified using our suggested model depending on classification rate and system performance.
- **Adaptive analysis:** The acquisition of EEG from NC subjects and AZD patients has varying patterns. The changes in the brain during AZD may slow down or increase the variations in electrical activities. Tracking these changes in the EEG with a predefined basis function may not yield desired system performance. Our adaptive and data-driven model has provided accurate analysis (higher accuracy) and synthesis (perfect reconstruction) with the help of an optimization algorithm.
- **Identification of channels and number of features:** EEG acquisition provides minute temporal information because of excellent temporal resolution. However, the spatial resolution of EEG signals is poor. To overcome this, acquisition of signals from multiple electrodes is performed. Also, researchers have used many features including statistical, nonlinear, time–frequency, and spectral features. The cost and time of computation rise when all available channels and features are used for analysis. We have presented a

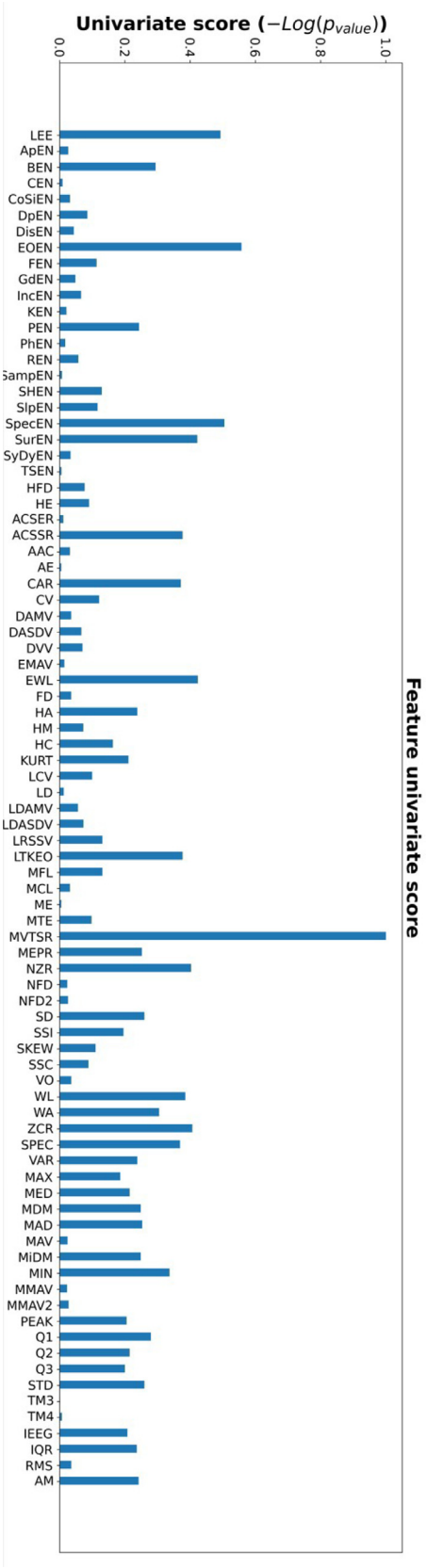

Fig. 5. Feature rank obtained using Univariate analysis.

method for determining the most important channel and the optimal number of features necessary to optimize system performance. It is important to highlight that when compared to a study of all channels and features at once, the performance of a single channel with optimal features reduced slightly.

- **Explainability:** Medical signal and image analysis has undergone tremendous change because of ML and DL. For image and signal-based AZD detection with the best system performance, several models have been devised. The lack of explainability in the decisions made by ML and DL models causes clinicians to express their unease with them, even after they have been successful in automating decision-making. Individuals can make local and global predictions using XAI when ML or DL models are developed. In our framework, we examined at the XBM model, which provides information about the prediction made throughout the model's training and testing. It educates users to obtain maximum performance, enhanced troubleshooting, higher trust, and strategies for overcoming bias and other bottlenecks.

The benefits and shortcomings of the proposed model are listed below:

- Our model is data-driven as do not require pre-defined basis function.
- The model offers limited computational complexity due to reduction in feature size from 1360 to 9.
- The model is accurate and robust as it is validated using holdout, LOSO, and 10-fold CV techniques.
- The developed model provides explanation of each/overall predictions which can be easily understood and debugged by clinicians.
- The developed Adazd-Net model is robust, adaptive, and simple as it is data-driven. It also yielded maximum performance, and explores channel/feature analysis.

The main limitation of this work is that we have used only single dataset comprising of 663 epochs belonging to 23 subjects.

6. Conclusion

We devised an automated, adaptable, accurate, and explainable model for detecting AZD with EEG signals. Our designed Adazd-Net model is ready to aid medical specialists in the detection and explanation of decisions. Our model adjusts automatically to the spontaneous fluctuations in the EEG signals of AZD and NC subjects. Our developed analysis tool not only provides accurate analysis by generating informative subbands but also yielded perfect reconstruction. Our model demonstrates that the frontal area, which is responsible for emotions, personality, motor movement, intelligence, and speech, is critical in the identification of AZD. Using 10-fold CV, holdout, and LOSO validation approaches, the proposed explainable model can detect the AZD with an ACCY of 99.85%, 98.51%, and 91.30%, respectively. The main limitation of this work is that we have used only 23 subjects to develop the adaptive XAI-based AZD detection model. In the future, we plan validate our model with huge database obtained from diverse races. Researchers may employ the combination of adaptive signal analysis, effective feature selection, and explainable predictions to detect various brain disorders and physiological changes.

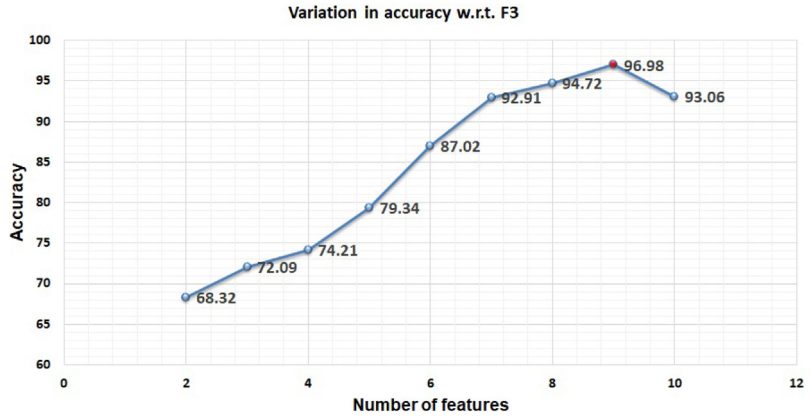

Fig. 6. Variation in accuracy (%) with number of features for F3 channel.

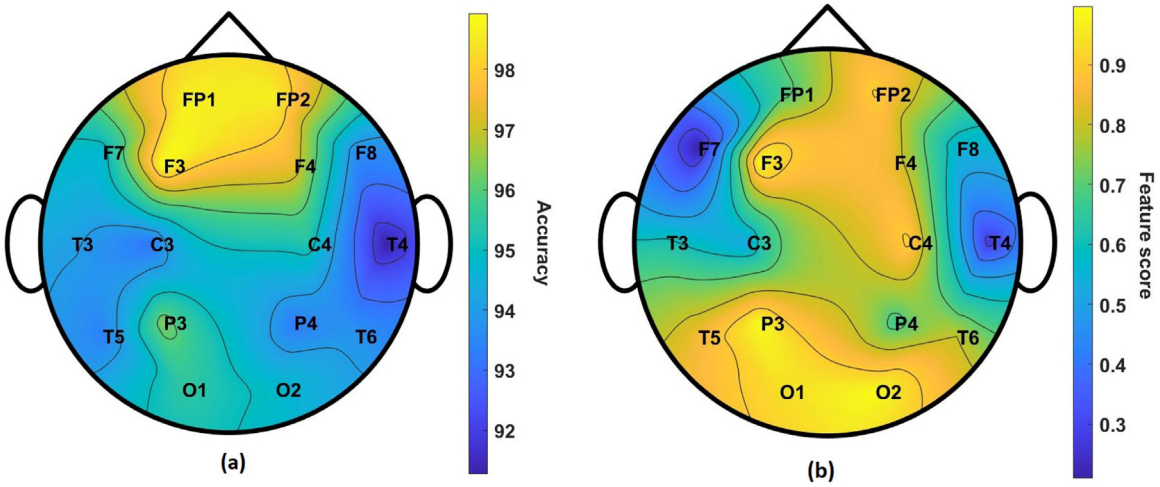

Fig. 7. Topographic maps obtained for our proposed Adazd-Net; (a) Accuracy, and (b) Feature score.

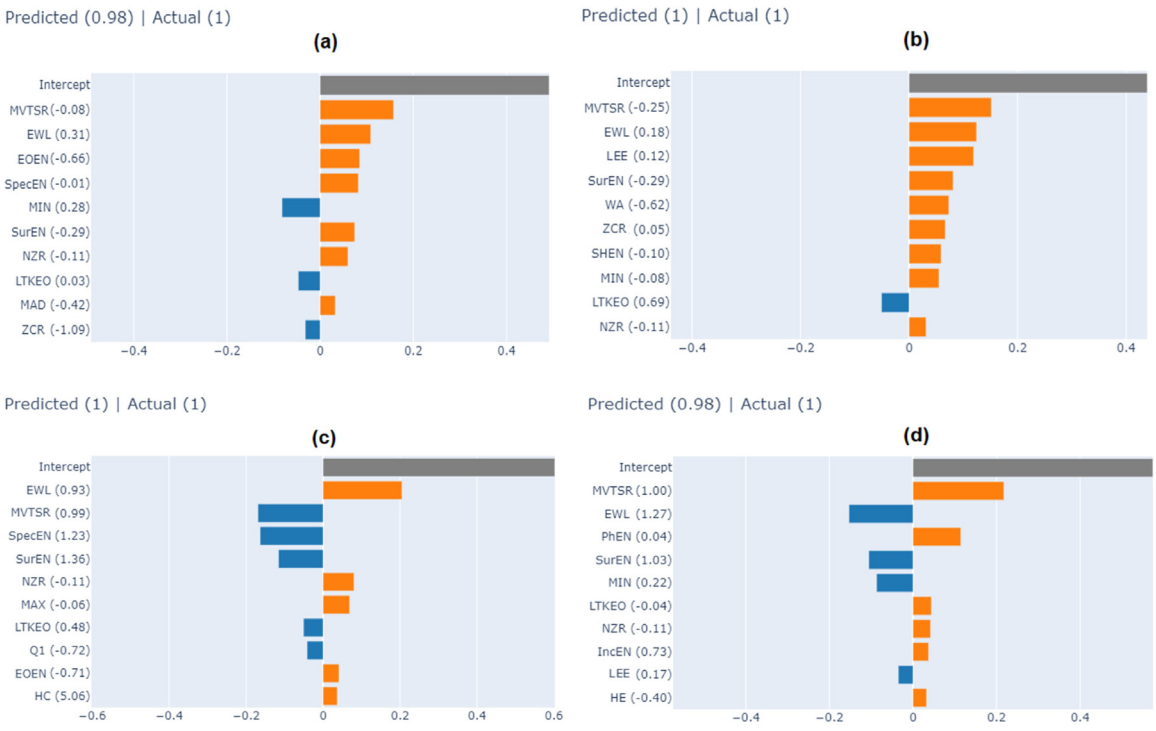

Fig. 8. Local explainability of individual predictions using LIME for features.

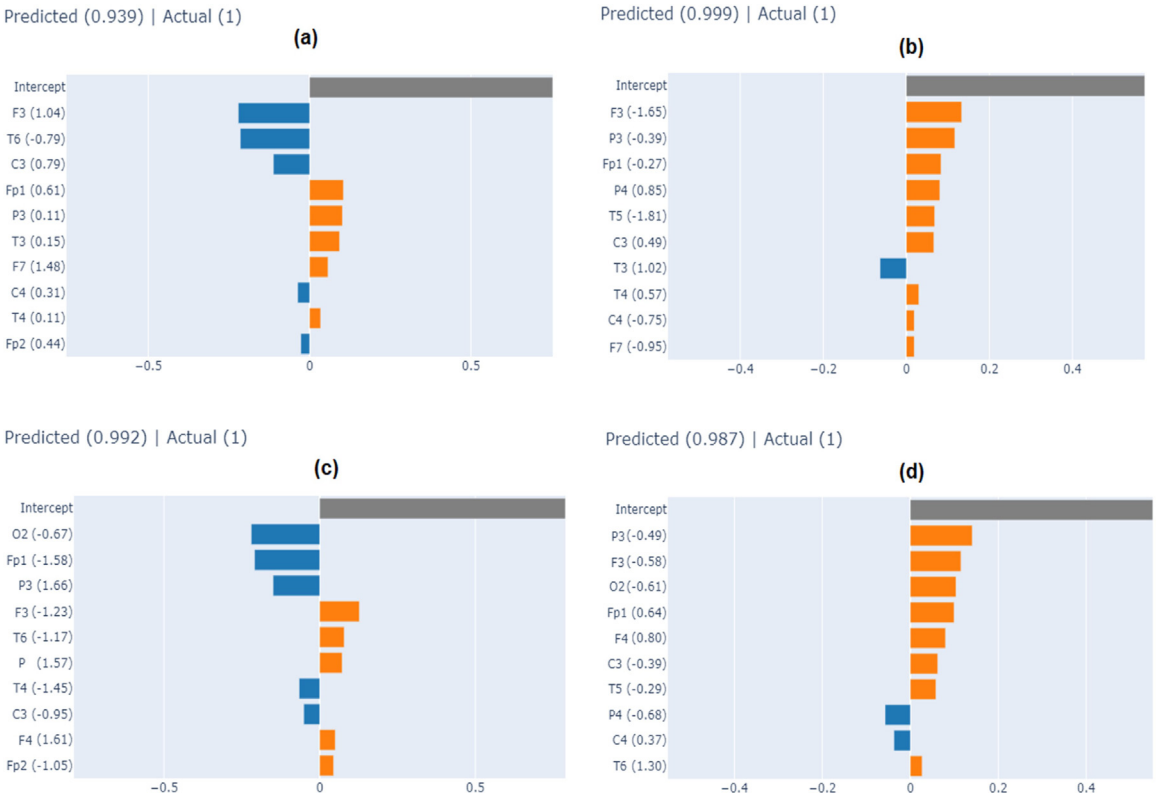

Fig. 9. Local explainability of individual predictions using LIME for channels.

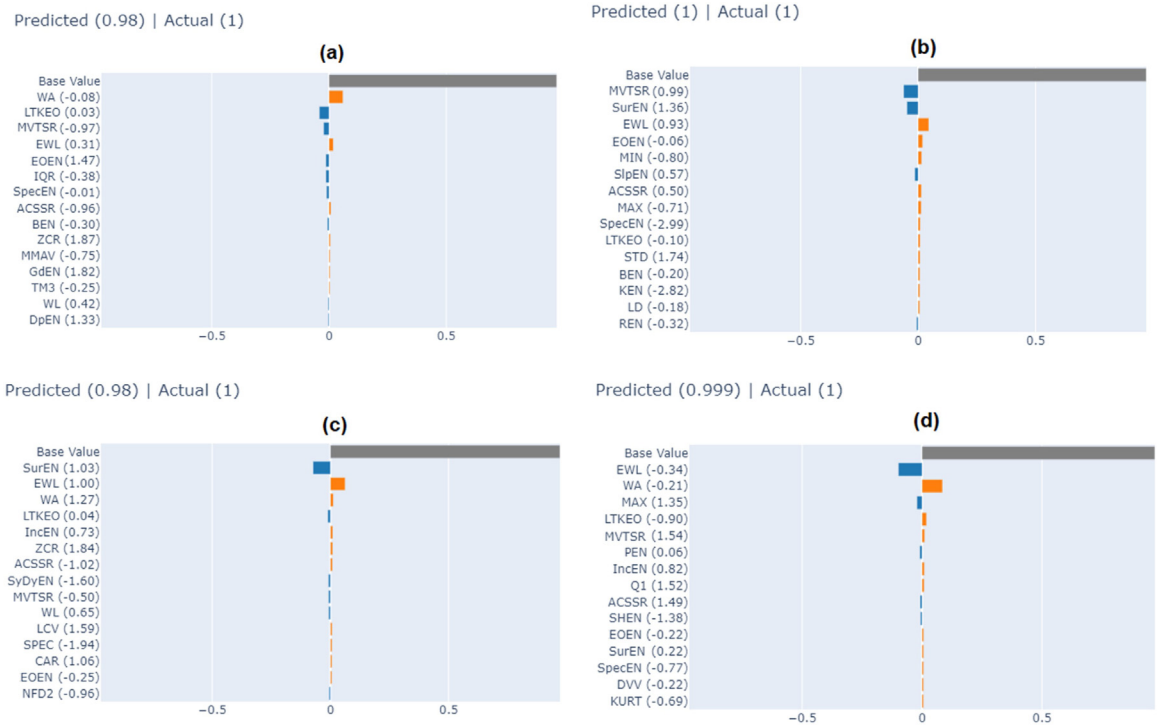

Fig. 10. Local explainability of individual predictions using SHAP for features.

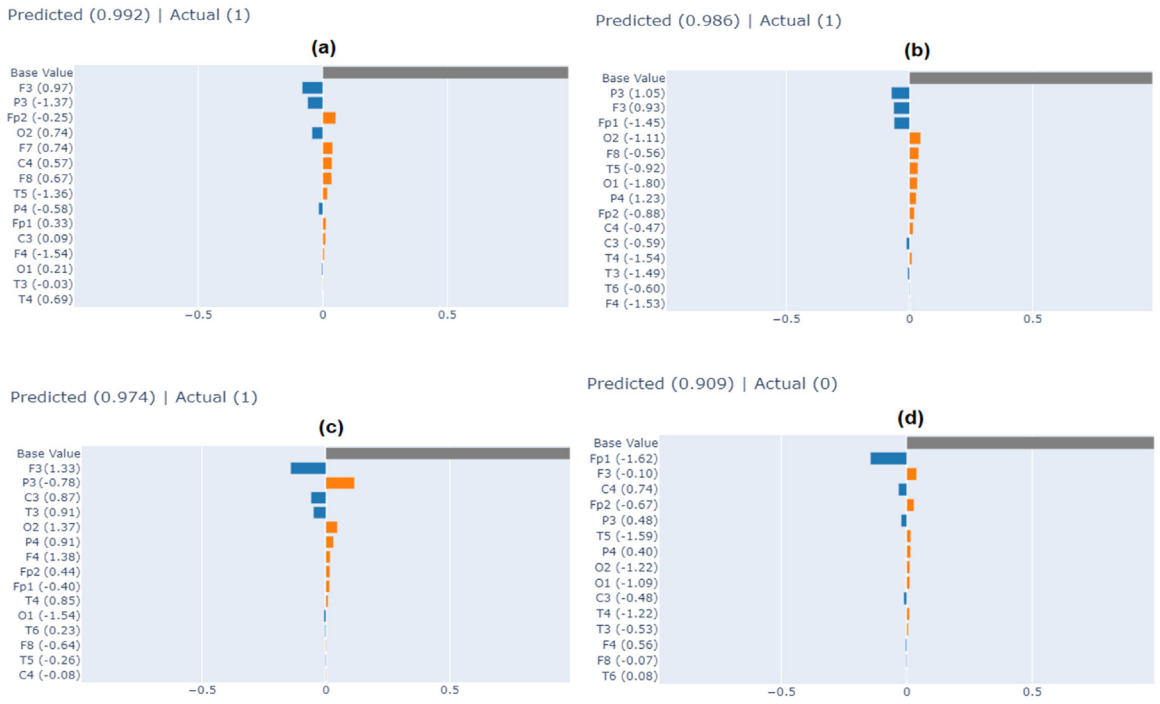

Fig. 11. Local explainability of individual predictions using SHAP for channels.

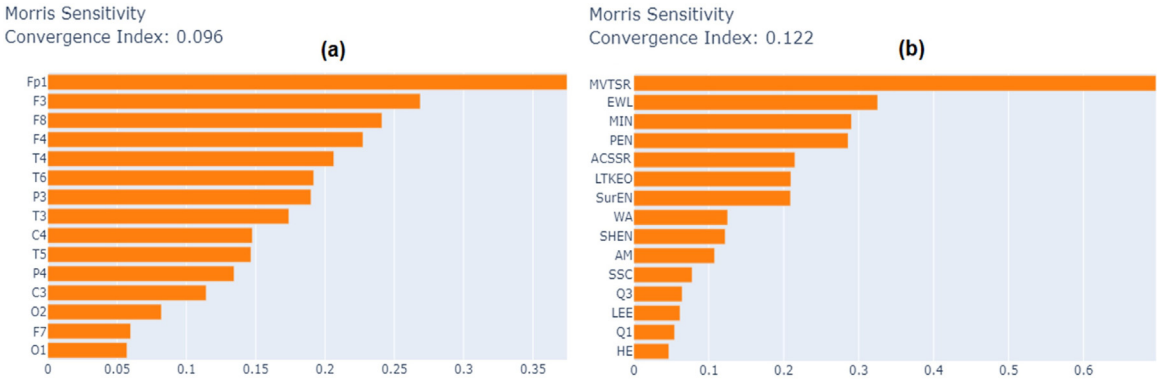

Fig. 12. Global explainability of model using MS (a) Channels and (b) Features.

Table 6
Performance comparison with existing SOTA using the same EEG dataset.

Authors (Year)	Feature Extraction	Classifier	Performance matrices				
			ACCY	SNSY	SPCY	PRCS	F1-score
Escudero et al. [14] (2006)	MSE	–	90.91	90.91	90.91	–	–
Abasolo et al. [18] (2006)	SpecEN and SHEN	–	77.27	63.64	90.91	–	–
Abasolo et al. [15] (2005)	ApEN	–	–	80	75	–	–
Abasolo et al. [16] (2008)	ApEN and AMI	–	90.91	100	81.82	–	–
Simons et al. [19] (2015)	QSE	–	77.27	–	–	–	–
Simons et al. [17] (2018)	FEN	–	86.36	90.91	81.82	–	–
Puri et al. [21] (2022)	TQWT and non-linear features	EBT (10-fold)	96.2	90.49	97.5	93.48	95.09
Puri et al. [22] (2022)	EMD and Hjorth parameter	LSSVM (10-fold)	92.9	94.32	94.34	94.33	94.32
Puri et al. [20] (2022)	SpecEN and KMC	SVM (10-fold)	95.6	95.2	–	95.2	95.1
Puri et al. [23] (2022)	WPA	SVM (10-fold)	97.5	97.08	97.45	–	–
Puri et al. [24] (2023)	LCOWFBs-v and non-linear features	SVM (10-fold)	98.6	97.34	99.8	–	–
Dogan et al. [27] (2022)	PBP and TQWT	KNN (10-fold)	100	100	100	–	–
Adazd-Net	**AFAWT**	**XBM (10-fold)**	99.85	99.75	100	100	99.88
		XBM (LOSO)	91.30	85.71	100	100	92.31
		XBM (Holdout)	98.51	100	96.88	97.29	98.63
		XBM (Brain Region)	99.25	98.86	99.24	99.25	99.37

CRediT authorship contribution statement

Smith K. Khare: Writing – original draft, Validation, Software, Methodology, Formal analysis, Conceptualization. **U. Rajendra Acharya:** Writing – review & editing, Visualization, Validation, Supervision, Investigation, Data curation.

Declaration of competing interest

The authors declare that they have no known competing financial interests or personal relationships that could have appeared to influence the work reported in this paper.

Data availability

Data will be made available on request.

Acknowledgment

The authors would like to acknowledge and thank the University of Valladolid for making the EEG dataset publicly available.

Funding

The authors declare that there is no funding received for this research.

Appendix A. Artificial hummingbird optimization algorithm

The AHOA works in following steps to get the optimal parameters for a cost function. The steps are initialization, guided foraging, territorial foraging, and migration foraging.

A.1. Initialization

During the initialization phase number of variables to be optimized, search agents, defining lower and upper bounds, and maximum number of iterations are defined. The AHOA is initialized to explore a search space within lower and upper bounds. The random initialization of hummingbirds with m population placed on k food sources are given by [47]

$$s_i = L_B + \rho(U_B - l_B) \tag{A.1}$$

where the position of ith food source that is the solution of a given problem is represented by s_i, lower and upper bounds are L_B and U_B and random vector ρ in range [0,1]. Further, the visit table of food sources is initialized using the following relation [47]

$$TV_{i,j} = \begin{cases} 0, & if\ i \neq j \\ \text{null}, & i = j \end{cases} \tag{A.2}$$

The $TV_{i,j}$ = null indicates hummingbird is consuming food at specific food source and $TV_{i,j}$ = 0 denotes the ith hummingbird has just visited the jth food source.

A.2. Guided foraging

The hummingbirds have a natural tendency to explore food source with highest nectar level indicating that a target food source must have a long unvisited time by that hummingbird and a high nectar-refilling rate. During foraging, three flying abilities are sufficiently utilized and modeled in the AHOA by providing a direction switch vector: omnidirectional, diagonal, and axial flights. The axial (hummingbird movement along any coordinate axis), diagonal (movement along diagonal from one corner to another corner of a rectangle), and omnidirectional (any flight direction can be projected to each of the three coordinate axes) flights for $d - D$ is defined as follows [47]

$$\begin{aligned} D^{(i)}_{axial} &= \begin{cases} 1, & i = randi([1, d]) \\ 0, & elsewhere \end{cases} \\ D^{(i)}_{diagonal} &= \begin{cases} 1, & i = P(j), \\ 0, & elsewhere \end{cases} \\ D^{(i)}_{omnidirectional} &= 1 \\ i &= 1, 2, \ldots., d \\ j \in [1, k], P &= randperm(k) \\ k \in [2, [r1.(d-2)] &+ 1] \end{aligned} \tag{A.3}$$

where random number $r1$ is (0,1), the function $randi([1, d])$ and $randperm(k)$ generates random integer between 1 to d and from 1 to k. It is noteworthy to mention that only master hummingbirds use axial and diagonal flights while other hummingbirds use omnidirectional flights. The hummingbird (search agents) obtain candidate food source i.e. possible solution and updation is performed from older food source to current food source (local best solution). The formulation of guided foraging behavior and a candidate food source is given by [47]

$$\begin{aligned} u_i(t+1) &= s_{i,tar}(t) + \alpha \cdot D \cdot (s_i(t) - s_{i,tar}(t)) \\ \alpha &\sim N(0, 1) \end{aligned} \tag{A.4}$$

where $s_{i,tar}$ indicates the target food source that ith hummingbird wish to visit, guided factor α is subjected to normal distribution $N(0, 1)$ having mean 0. The updation in position of ith food source is modeled using [47]

$$s_i(t+1) = \begin{cases} s_i(t), & g(s_i(t)) < g(u_i(t+1)) \\ u_i(t+1), & g(s_i(t)) > g(u_i(t+1)) \end{cases} \tag{A.5}$$

where $g(\cdot)$ is a fitness function value denoting RMSD.

A.3. Territorial foraging

Once the nectar of current food source is consumed by hummingbird, it search for new source in its neighboring region of own territory for a better food source than current one (new local best). The formulation of local search of hummingbirds in the territorial foraging strategy and a candidate food source is given by [47]

$$\begin{aligned} u_i(t+1) &= s_i(t) + b \cdot D \cdot s_i(t) \\ b &\sim N(0, 1) \end{aligned} \tag{A.6}$$

where the territorial factor b subjecting to normal distribution with zero mean.

A.4. Migration foraging

Typically, repeated visits to food sources result in a scarcity of food, causing the hummingbird to migrate to a distant food source to feed. This is known as migratory foraging, and it is performed through the use of the migration coefficient in AHOA. If the number of iterations exceeds the migrating coefficient, the hummingbird will migrate to a new search space generated at random from the whole search space. The migrating foraging of hummingbird is given by [47]

$$s_{wor}(t+1) = L_B + \rho(U_B - l_B) \tag{A.7}$$

Table B.7
List of nonlinear features and their abbreviations.

Features	Abbreviations
Higuchi fractal dimension	HFD
Hurst exponent	HE
Absolute value of the summation of exponential root	ACSER
Absolute value of the summation of square root	ACSSR
Average amplitude change	AAC
Lyapunov exponent	LE
Cardinality	CAR
Coefficient of variation	CV
Difference absolute mean value	DAMV
Difference absolute standard deviation value	DASDV
Difference variance value	DVV
Enhanced mean absolute value	EMAV
Enhanced wavelength	EWL
First difference	FD
Hjorth mobility	HM
Hjorth complexity	HC
Katz fractal dimension	KFD
Kurtosis	KURT
Log coefficient of variation	LCV
Log detector	LD
Log difference absolute mean value	LDAMV
Log difference absolute standard deviation value	LMASDV
Log root sum of sequential variation	LRSSV
Log teager kaiser energy operator	LKTEO
Maximum fractal length	MFL
Mean curve length	MCL
Mean energy	ME
Mean teager energy	MTE
Mean value of the square root	MVTSR
Encephalopulse percentage rate	MEPR
New zero crossing rate	NZR
Normalized first difference	NFD
Normalized second difference	NFD2
Second difference	SD
Simple square integral	SSI
Skewness	SKEW
Slope sign change	SSC
V Order	VO
Waveform length	WL
Willison Amplitude	WA
Zero crossing rate	ZCR
Spectral flatness	SPEC

where s_{wor} is the food source with the worst nectar-refilling rate in the population. The Matlab toolbox for AHOA is publicly available at https://seyedalimirjalili.com/aha. Thus, the optimization provides local solution in each iteration using search agents. After each iteration, the local best is compared with the previous local best. If it is better than the previous one it is updated, if it is not, the previous solution is retained which is continued till the final iteration to get the global best solution.

Appendix B. Nonlinear features

See Table B.7.

Appendix C. Entropy features

See Table C.8.

Appendix D. Statistical features

See Table D.9.

Table C.8
List of entropy features and their abbreviations.

Features	Abbreviations
Log energy entropy	LEE
Approximate entropy	ApEN
Bubble entropy	BubbEN
Conditional entropy	CondEN
Cosine similarity entropy	CoSiEN
Display entropy	DispEN
Distance entropy	DistEN
Entropy of entropy	EOEN
Fuzzy entropy	FEN
Gridded distribution entropy	GridEN
Incremental entropy	IncrEN
Kolmogorov entropy	KEN
Permutation entropy	PEN
Phase entropy	PhaseEN
Renyi entropy	REN
Sample entropy	SampEN
Shannon entropy	SHEN
Slope entropy	SlpEN
Spectral entropy	SpecEN
SURE entropy	SurEN
symbolic dynamic entropy	SyDyEN
Tsallis entropy	TSEN

Table D.9
List of statistical features and their abbreviations.

Features	Abbreviations
Variance	VAR
Maxima	MAX
Median	MED
Maximum deviation from mean	MDM
Mean absolute deviation	MAD
Mean absolute value	MAV
Minimum deviation from mean	MiDM
Minima	MIN
Modified mean absolute value	MMAV
Modified mean absolute value 2	MMAV2
Peak value	PEAK
First quantile	Q1
Second quantile	Q2
Third quantile	Q3
Standard deviation	STD
Third temporal moment	TM3
Fourth temporal moment	TM4
Integral EEG	IEEG
Interquartile range	IQR
Root mean square value	RMS
Arithmetic mean	AM

References

[1] J.L. Podcasy, C.N. Epperson, Considering sex and gender in Alzheimer disease and other dementias, Dialogues Clin. Neurosci. (2022).

[2] A. Nandi, N. Counts, S. Chen, B. Seligman, D. Tortorice, D. Vigo, D.E. Bloom, Global and regional projections of the economic burden of Alzheimer's disease and related dementias from 2019 to 2050: A value of statistical life approach, EClinicalMedicine 51 (2022) 101580.

[3] Alzheimer's disease and healthy aging, 2022, https://www.cdc.gov/aging/index.html. (Accessed: 08 Nov 2022).

[4] Diagnosing Alzheimer's: How Alzheimer's is diagnosed, 2022, https://www.mayoclinic.org/diseases-conditions/alzheimers-disease/in-depth/alzheimers/art-20048075. (Accessed: 08 Nov 2022).

[5] X. Zhao, C.K.E. Ang, U.R. Acharya, K.H. Cheong, Application of artificial intelligence techniques for the detection of Alzheimer's disease using structural MRI images, Biocybern. Biomed. Eng. 41 (2) (2021) 456–473, http://dx.doi.org/10.1016/j.bbe.2021.02.006.

[6] P.L. McGeer, Brain imaging in Alzheimer's disease, Br. Med. Bull. 42 (1) (1986) 24–28, http://dx.doi.org/10.1093/oxfordjournals.bmb.a072093.

[7] M. Ouchani, S. Gharibzadeh, M. Jamshidi, M. Amini, A review of methods of diagnosis and complexity analysis of Alzheimer's disease using EEG signals, BioMed. Res. Int. 2021 (2021).

[8] S.K. Khare, V. Bajaj, S. Taran, G. Sinha, 1 - multiclass sleep stage classification using artificial intelligence based time-frequency distribution

and CNN, in: V. Bajaj, G. Sinha (Eds.), Artificial Intelligence-Based Brain-Computer Interface, Academic Press, 2022, pp. 1–21, http://dx.doi.org/10.1016/B978-0-323-91197-9.00012-6.

[9] S.K. Khare, N.B. Gaikwad, V. Bajaj, VHERS: A novel variational mode decomposition and Hilbert transform-based EEG rhythm separation for automatic ADHD detection, IEEE Trans. Instrum. Meas. 71 (2022) 1–10, http://dx.doi.org/10.1109/TIM.2022.3204076.

[10] S.K. Khare, V. Bajaj, U.R. Acharya, PDCNNet: An automatic framework for the detection of Parkinson's disease using EEG signals, IEEE Sens. J. 21 (15) (2021) 17017–17024, http://dx.doi.org/10.1109/JSEN.2021.3080135.

[11] B. Ari, N. Sobahi, Ö.F. Alçin, A. Sengur, U. Acharya, Accurate detection of autism using douglas-peucker algorithm, sparse coding based feature mapping and convolutional neural network techniques with EEG signals, Comput. Biol. Med. 143 (2022) 105311, http://dx.doi.org/10.1016/j.compbiomed.2022.105311.

[12] E. Perez-Valero, J. Minguillon, C. Morillas, F. Pelayo, M.A. Lopez-Gordo, Detection of Alzheimer's disease using a four-channel EEG montage, in: International Work-Conference on the Interplay Between Natural and Artificial Computation, Springer, 2022, pp. 436–445.

[13] T. Wu, F. Sun, Y. Guo, M. Zhai, S. Yu, J. Chu, C. Yu, Y. Yang, Spatio-temporal dynamics of entropy in EEGS during music stimulation of Alzheimer's disease patients with different degrees of dementia, Entropy 24 (8) (2022) http://dx.doi.org/10.3390/e24081137.

[14] J. Escudero, D. Abásolo, R. Hornero, P. Espino, M. López, Analysis of electroencephalograms in Alzheimer's disease patients with multiscale entropy, Physiol. Meas. 27 (11) (2006) 1091.

[15] D. Abásolo, R. Hornero, P. Espino, J. Poza, C.I. Sánchez, R. de la Rosa, Analysis of regularity in the EEG background activity of Alzheimer's disease patients with approximate entropy, Clin. Neurophysiol. 116 (8) (2005) 1826–1834, http://dx.doi.org/10.1016/j.clinph.2005.04.001, https://www.sciencedirect.com/science/article/pii/S1388245705001331.

[16] D. Abásolo, J. Escudero, R. Hornero, C. Gómez, P. Espino, Approximate entropy and auto mutual information analysis of the electroencephalogram in Alzheimer's disease patients, Med. Biol. Eng. Comput. 46 (2008) 1019–1028.

[17] S. Simons, P. Espino, D. Abásolo, Fuzzy entropy analysis of the electroencephalogram in patients with Alzheimer's disease: Is the method superior to sample entropy? Entropy 20 (1) (2018) http://dx.doi.org/10.3390/e20010021.

[18] D. Abásolo, R. Hornero, P. Espino, D. Alvarez, J. Poza, Entropy analysis of the EEG background activity in Alzheimer's disease patients, Physiol. Meas. 27 (3) (2006) 241.

[19] S. Simons, D. Abasolo, J. Escudero, Classification of Alzheimer's disease from quadratic sample entropy of electroencephalogram, Healthcare Technol. Lett. 2 (3) (2015) 70–73, http://dx.doi.org/10.1049/htl.2014.0106, arXiv:https://ietresearch.onlinelibrary.wiley.com/doi/pdf/10.1049/htl.2014.0106.

[20] D. Puri, S. Nalbalwar, A. Nandgaonkar, A. Wagh, EEG based diagnosis of Alzheimer's disease using Kolmogorov complexity, in: Applied Information Processing Systems, Springer, 2022, pp. 157–165.

[21] D. Puri, S. Nalbalwar, A. Nandgaonkar, A. Wagh, Alzheimer's disease detection from optimal electroencephalogram channels and tunable Q-wavelet transform, Indo. J. Elec. Engg. Comp. Sci 25 (3) (2022) 1420–1428.

[22] D. Puri, S. Nalbalwar, A. Nandgaonkar, P. Kachare, J. Rajput, A. Wagh, Alzheimer's disease detection using empirical mode decomposition and Hjorth parameters of EEG signal, in: 2022 International Conference on Decision Aid Sciences and Applications, DASA, 2022, pp. 23–28, http://dx.doi.org/10.1109/DASA54658.2022.9765111.

[23] D. Puri, S. Nalbalwar, A. Nandgaonkar, A. Wagh, Alzheimer's disease detection with optimal EEG channel selection using wavelet transform, in: 2022 International Conference on Decision Aid Sciences and Applications, DASA, 2022, pp. 443–448, http://dx.doi.org/10.1109/DASA54658.2022.9765166.

[24] D.V. Puri, S.L. Nalbalwar, A.B. Nandgaonkar, J.P. Gawande, A. Wagh, Automatic detection of Alzheimer's disease from EEG signals using low-complexity orthogonal wavelet filter banks, Biomed. Signal Process. Control 81 (2023) 104439, http://dx.doi.org/10.1016/j.bspc.2022.104439, https://www.sciencedirect.com/science/article/pii/S174680942200893X.

[25] R. Cassani, T.H. Falk, F.J. Fraga, M. Cecchi, D.K. Moore, R. Anghinah, Towards automated electroencephalography-based Alzheimer's disease diagnosis using portable low-density devices, Biomed. Signal Process. Control 33 (2017) 261–271.

[26] R. Cassani, T.H. Falk, Automated Alzheimer's disease diagnosis using a low-density EEG layout and new features based on the power of modulation spectral patches, in: 2019 IEEE International Conference on Systems, Man and Cybernetics, SMC, 2019, pp. 1259–1263, http://dx.doi.org/10.1109/SMC.2019.8914540.

[27] S. Dogan, M. Baygin, B. Tasci, H.W. Loh, P.D. Barua, T. Tuncer, R.-S. Tan, U.R. Acharya, Primate brain pattern-based automated Alzheimer's disease detection model using EEG signals, Cogn. Neurodyn. (2022) 1–13.

[28] K. AlSharabi, Y. Bin Salamah, A.M. Abdurraqeeb, M. Aljalal, F.A. Alturki, EEG signal processing for Alzheimer's disorders using discrete wavelet transform and machine learning approaches, IEEE Access 10 (2022) 89781–89797, http://dx.doi.org/10.1109/ACCESS.2022.3198988.

[29] Y. Ding, Y. Chu, M. Liu, Z. Ling, S. Wang, X. Li, Y. Li, Fully automated discrimination of Alzheimer's disease using resting-state electroencephalography signals, Quant. Imaging Med. Surg. 12 (2) (2022) 1063.

[30] K. Li, J. Wang, S. Li, H. Yu, L. Zhu, J. Liu, L. Wu, Feature extraction and identification of Alzheimer's disease based on latent factor of multi-channel EEG, IEEE Trans. Neural Syst. Rehabil. Eng. 29 (2021) 1557–1567, http://dx.doi.org/10.1109/TNSRE.2021.3101240.

[31] D. Pirrone, E. Weitschek, P. Di Paolo, S. De Salvo, M.C. De Cola, EEG signal processing and supervised machine learning to early diagnose Alzheimer's disease, Appl. Sci. 12 (11) (2022) http://dx.doi.org/10.3390/app12115413.

[32] H. Yu, X. Lei, Z. Song, C. Liu, J. Wang, Supervised network-based fuzzy learning of EEG signals for Alzheimer's disease identification, IEEE Trans. Fuzzy Syst. 28 (1) (2020) 60–71, http://dx.doi.org/10.1109/TFUZZ.2019.2903753.

[33] M. Alessandrini, G. Biagetti, P. Crippa, L. Falaschetti, S. Luzzi, C. Turchetti, EEG-based Alzheimer's disease recognition using robust-PCA and LSTM recurrent neural network, Sensors 22 (10) (2022) http://dx.doi.org/10.3390/s22103696.

[34] A.M. Alvi, S. Siuly, M.C. De Cola, H. Wang, DRAM-Net: A deep residual Alzheimer's diseases and mild cognitive impairment detection network using EEG data, in: International Conference on Health Information Science, Springer, 2022, pp. 42–53.

[35] C.L. Alves, A.M. Pineda, K. Roster, C. Thielemann, F.A. Rodrigues, EEG functional connectivity and deep learning for automatic diagnosis of brain disorders: Alzheimer's disease and schizophrenia, J. Phys.: Complexity 3 (2) (2022) 025001, http://dx.doi.org/10.1088/2632-072X/ac5f8d.

[36] D. Komolovaitė, R. Maskeliūnas, R. Damaševičius, Deep convolutional neural network-based visual stimuli classification using electroencephalography signals of healthy and Alzheimer's disease subjects, Life 12 (3) (2022) http://dx.doi.org/10.3390/life12030374.

[37] A.M. Alvi, S. Siuly, H. Wang, A long short-term memory based framework for early detection of mild cognitive impairment from EEG signals, IEEE Trans. Emerg. Top. Comput. Intell. (2022) 1–14, http://dx.doi.org/10.1109/TETCI.2022.3186180.

[38] M. Amini, M.M. Pedram, A. Moradi, M. Ouchani, Diagnosis of Alzheimer's disease by time-dependent power spectrum descriptors and convolutional neural network using EEG signal, Comput. Math. Methods Med. 2021 (2021).

[39] S. Fouladi, A.A. Safaei, N. Mammone, F. Ghaderi, M. Ebadi, Efficient deep neural networks for classification of Alzheimer's disease and mild cognitive impairment from scalp EEG recordings, Cogn. Comput. (2022) 1–22.

[40] Z. Song, B. Deng, J. Wang, G. Yi, An EEG-based systematic explainable detection framework for probing and localizing abnormal patterns in Alzheimer's disease, J. Neural Eng. 19 (3) (2022) 036007, http://dx.doi.org/10.1088/1741-2552/ac697d.

[41] X. Bi, H. Wang, Early Alzheimer's disease diagnosis based on EEG spectral images using deep learning, Neural Netw. 114 (2019) 119–135, http://dx.doi.org/10.1016/j.neunet.2019.02.005.

[42] C.J. Huggins, J. Escudero, M.A. Parra, B. Scally, R. Anghinah, A.V.L.D. Araújo, L.F. Basile, D. Abasolo, Deep learning of resting-state electroencephalogram signals for three-class classification of Alzheimer's disease, mild cognitive impairment and healthy ageing, J. Neural Eng. 18 (4) (2021) 046087, http://dx.doi.org/10.1088/1741-2552/ac05d8.

[43] W. Xia, R. Zhang, X. Zhang, M. Usman, A novel method for diagnosing Alzheimer's disease using deep pyramid CNN based on EEG signals, Heliyon 9 (4) (2023) e14858, http://dx.doi.org/10.1016/j.heliyon.2023.e14858, https://www.sciencedirect.com/science/article/pii/S2405844023020650.

[44] S.-A. Sadegh-Zadeh, E. Fakhri, M. Bahrami, E. Bagheri, R. Khamsehashari, M. Noroozian, A.M. Hajiyavand, An approach toward artificial intelligence Alzheimer's disease diagnosis using brain signals, Diagnostics 13 (3) (2023) http://dx.doi.org/10.3390/diagnostics13030477, https://www.mdpi.com/2075-4418/13/3/477.

[45] Y. Hong, T. Jeong, U. Park, D. Kim, Y.C. Youn, H.-J. Kim, S. Choi, J. Jeong, S. Yoon, K. Park, E.-J. Kim, B. Yoon, J.W. Jang, J. Hong, J.-Y. Lee, S. Kang, Identifying Alzheimer's disease dementia through ensemble learning of channel and source level electroencephalogram features, 2023, http://dx.doi.org/10.21203/rs.3.rs-2801213/v1, ResearchSquare Preprint.

[46] H.W. Loh, C.P. Ooi, S. Seoni, P.D. Barua, F. Molinari, U.R. Acharya, Application of explainable artificial intelligence for healthcare: A systematic review of the last decade (2011–2022), Comput. Methods Programs Biomed. 226 (2022) 107161, http://dx.doi.org/10.1016/j.cmpb.2022.107161, https://www.sciencedirect.com/science/article/pii/S0169260722005429.

[47] W. Zhao, L. Wang, S. Mirjalili, Artificial hummingbird algorithm: A new bio-inspired optimizer with its engineering applications, Comput. Methods Appl. Mech. Engrg. 388 (2022) 114194, http://dx.doi.org/10.1016/j.cma.2021.114194.

[48] Y. Lou, R. Caruana, J. Gehrke, G. Hooker, Accurate intelligible models with pairwise interactions, in: Proceedings of the 19th ACM SIGKDD International Conference on Knowledge Discovery and Data Mining, KDD '13, Association for Computing Machinery, New York, NY, USA, 2013, pp. 623–631, http://dx.doi.org/10.1145/2487575.2487579.

[49] S.K. Khare, S. March, P.D. Barua, V.M. Gadre, U.R. Acharya, Application of data fusion for automated detection of children with developmental and mental disorders: A systematic review of the last decade, Inf. Fusion 99 (2023) 101898, http://dx.doi.org/10.1016/j.inffus.2023.101898, https://www.sciencedirect.com/science/article/pii/S1566253523002142.

[50] K. Smith, D. Abásolo, J. Escudero, Accounting for the complex hierarchical topology of EEG phase-based functional connectivity in network binarisation, PLoS One 12 (10) (2017) e0186164.

[51] M.F. Folstein, S.E. Folstein, P.R. McHugh, "Mini-mental state": A practical method for grading the cognitive state of patients for the clinician, J. Psychiatr. Res. 12 (3) (1975) 189–198, http://dx.doi.org/10.1016/0022-3956(75)90026-6.

[52] K. Smith, Data for 'accounting for the complex hierarchical topology of EEG phase-based functional connectivity in network binarisation', 2017, https://osf.io/jbysn/.

[53] M. Sharma, R.B. Pachori, U.R. Acharya, A new approach to characterize epileptic seizures using analytic time-frequency flexible wavelet transform and fractal dimension, Pattern Recognit. Lett. 94 (2017) 172–179.

[54] C. Sravani, V. Bajaj, S. Taran, A. Sengur, Flexible analytic wavelet transform based features for physical action identification using sEMG signals, IRBM 41 (1) (2020) 18–22, http://dx.doi.org/10.1016/j.irbm.2019.07.002.

[55] I. Bayram, An analytic wavelet transform with a flexible time-frequency covering, IEEE Trans. Signal Process. 61 (5) (2012) 1131–1142.

[56] M.W. Flood, B. Grimm, EntropyHub: An open-source toolkit for entropic time series analysis, in: M. Rezakazemi (Ed.), PLOS ONE 16 (11) (2021) e0259448, http://dx.doi.org/10.1371/journal.pone.0259448.

[57] J. Too, A. Abdullah, N.M. Saad, W. Tee, EMG feature selection and classification using a pbest-guide binary particle swarm optimization, Computation 7 (1) (2019) 12, http://dx.doi.org/10.3390/computation.

[58] J. Too, A. Rahim, N. Mohd, Classification of hand movements based on discrete wavelet transform and enhanced feature extraction, Int. J. Adv. Comput. Sci. Appl. 10 (6) (2019) http://dx.doi.org/10.14569/ijacsa.2019.0100612.

[59] V.K. Sudarshan, U. Acharya, S.L. Oh, M. Adam, J.H. Tan, C.K. Chua, K.P. Chua, R.S. Tan, Automated diagnosis of congestive heart failure using dual tree complex wavelet transform and statistical features extracted from 2s of ECG signals, Comput. Biol. Med. 83 (2017) 48–58, http://dx.doi.org/10.1016/j.compbiomed.2017.01.019.

[60] M. Baygin, P.D. Barua, S. Dogan, T. Tuncer, S. Key, U.R. Acharya, K.H. Cheong, A hand-modeled feature extraction-based learning network to detect grasps using sEMG signal, Sensors 22 (5) (2022) http://dx.doi.org/10.3390/s22052007.

[61] H. Yaacob, F. Hossain, S. Shari, S.K. Khare, C.P. Ooi, U. Rajendra Acharya, Application of artificial intelligence techniques for brain-computer interface in mental fatigue detection: A systematic review (2011–2022), IEEE Access (2023) 1, http://dx.doi.org/10.1109/ACCESS.2023.3296382.

[62] M.T. Ribeiro, S. Singh, C. Guestrin, "Why should I trust you?": Explaining the predictions of any classifier, in: Proceedings of the 22nd ACM SIGKDD International Conference on Knowledge Discovery and Data Mining, KDD '16, Association for Computing Machinery, New York, NY, USA, 2016, pp. 1135–1144, http://dx.doi.org/10.1145/2939672.2939778.

[63] S.M. Lundberg, S.-I. Lee, A unified approach to interpreting model predictions, in: Proceedings of the 31st International Conference on Neural Information Processing Systems, NIPS '17, Curran Associates Inc., Red Hook, NY, USA, 2017, pp. 4768–4777.

[64] M.D. Morris, Factorial sampling plans for preliminary computational experiments, Technometrics 33 (2) (1991) 161–174.

[65] J. Herman, W. Usher, SALib: An open-source python library for sensitivity analysis, J. Open Source Softw. 2 (2017) http://dx.doi.org/10.21105/joss.00097.

[66] Lobes of the brain, 2022, https://qbi.uq.edu.au/brain/brain-anatomy/lobes-brain. (Accessed: 08 Nov 2022).